Journal of the Audio Engineering Society
Vol. 65, No. 1/2, January/February 2017 (© 2017)
DOI: https://doi.org/10.17743/jaes.2016.0057

Wave-Based Room Acoustics Simulation: Explicit/Implicit Finite Volume Modeling of Viscothermal Losses and Frequency-Dependent Boundaries

STEFAN BILBAO, *AES Associate Member,* **AND BRIAN HAMILTON**
(sbilbao@staffmail.ed.ac.uk) (brian.hamilton@ed.ac.uk)

Acoustics and Audio Group, University of Edinburgh, Edinburgh, United Kingdom

Time domain wave-based methods sidestep the simplifying hypotheses underlying geometric (ray-based) methods and offer, in theory, a complete solution to the problem of room acoustics simulation. Many issues remain at the level of algorithm design, particularly under realistic room configurations. The main design criteria are: (a) arbitrary room geometry, (b) general passive frequency-dependent and spatially-varying wall conditions, and (c) adequate modeling of viscothermal and relaxation effects. The third feature, which is the focus of this article, plays a major role in room decay times, particularly in the high frequency range. The main difficulty, under such general conditions, is in the construction of simulation methods that are numerically stable. Finite volume time domain (FVTD) methods generalize certain finite difference time domain (FDTD) methods, while allowing for such stability analysis. Here, FVTD methods under frequency-dependent impedance boundary conditions are extended to handle such viscothermal effects with an implicit/explicit time integration scheme, while allowing for a means of terminating a numerical method in a stable manner. An energy-based analysis of numerical stability is presented here in detail, leading to conditionally and unconditionally stable forms, and extended to cover the case of dissipation through a time-integrated energy balance. Simulation results are presented.

0 INTRODUCTION

Time-domain wave-based numerical techniques offer, at least in theory, a complete solution to the problem of room acoustics simulation, whether the application is to concert hall design, auralization, or artificial reverberation design. Such methods, for which the acoustic field is computed in its entirety over the room interior, rely on fewer simplifying hypotheses than geometric (or ray-based) methods; diffraction effects, in particular, are a natural byproduct of a wave-based simulation approach. For a recent elaboration of the distinctions between ray-based and wave-based simulation methods, see the review article [1]. Though computationally costly, recent advances in computing power allow for operation at audio rates and for room sizes approaching that of the concert hall [2, 3].

This article is concerned with time-domain wave-based simulation methods for a complete room acoustics problem, which must necessarily consist of the following realistic attributes:

- A realistic and non-trivial room geometry;
- General frequency-dependent and spatially-varying passive wall conditions;
- Wave propagation over the room interior including frequency-dependent sound absorption in air.

In the context of room acoustics, the most straightforward time domain technique is almost certainly the finite difference time domain (FDTD) method on a regular Cartesian grid, in the second-order form for the wave equation [4, 5], or in the interleaved first-order system adapted to acoustics from the electromagnetics literature [6, 7]. There are many varieties of such schemes, operating over different regular grid arrangements, and selecting different collections of neighbouring values—see, e.g., [8–10]. Time-stepping spectral methods operating over domains that have been decomposed into rectangular sub-regions comprise an alternative approach [11, 12].

A major issue underlying the construction of time-stepping methods is the determination of conditions for numerical stability. Methods for which rigorous stability conditions are currently unavailable (e.g., [11, 12]) carry the risks of exponential solution growth, which ultimately

places limitations on their reliability in a practical setting. Stability analysis is a relatively straightforward matter in the case of lossless wave propagation in unbounded free space, through, e.g., frequency-domain techniques such as von Neumann analysis [13], but when more realistic features of room acoustics (such as those listed above) are introduced, such techniques are limited in use. In particular, with regard to the first attribute listed above, although extensions of frequency-domain analysis are available under certain simple boundary conditions (such as, e.g., a straight wall or a single box-shaped domain [14, 15]), they do not easily extend to more realistic geometries. The introduction of frequency-dependent wall conditions leads to new complications in terms of stability analysis, particularly in the case of spatially-varying wall conditions.

In recent work [16, 17], the present authors have proposed a framework for the construction of time-domain wave-based schemes allowing for stability under the first two attributes listed above. This framework is based on an extension of finite volume time domain methods (FVTD) [7, 18], which naturally operate over unstructured grids, allowing for fine-grained modeling of detailed wall conditions and geometries. Furthermore, these FVTD methods reduce to certain FDTD methods when defined over regular, structured grids [16], allowing for efficient parallel implementations [3, 19]. The determination of sufficient stability conditions for arbitrary geometries and arbitrary passive wall terminations follows from energy-based analysis. Such an approach produces full-bandwidth results in realistic, non-trivial room geometries, under frequency-dependent wall conditions. An additional feature of interest is that using unstructured grids over the room boundary, compared with staircase termination, allows for much more accurate modeling of room modes and T_{60} decay times, as well as greater coherence of computed reflections [17].

One important feature of room acoustics modeling that has seen relatively little exploration, particularly in the context of wave-based simulation methods, is the third mentioned above: the effect of losses due to viscothermal and relaxation effects, leading to frequency-dependent decay in free space [20–22]. Such effects cannot be ignored, particularly in large spaces, otherwise calculated impulse responses or auralizations will be unnaturally "ringy." Such a model, however, introduces additional complexity to any resulting scheme and, in particular, leads to interaction with frequency-dependent conditions over irregular domains. The purpose of the present study is to extend the finite volume time domain approaches developed in [16, 19, 17] to include such viscothermal effects, and implicit time-integration, and to find suitable numerical stability conditions for such schemes, again over highly nontrivial wall terminations. This article is an extended version of a paper presented recently at the 60th Audio Engineering Society Conference in Leuven, Belgium [23].

The model equations and a suitable simplification for room acoustics appear in Sec. 1 including viscothermal losses and a spatially-varying and frequency-dependent wall condition generalizing that which appears in [23]. An energy-balanced formulation relates stored energy over the room interior and at the boundary to time integrated power loss, again over the room interior through viscothermal damping, and at the room boundary. Finite volume discretization techniques are described in Sec. 2, and a two-parameter family of explicit/implicit schemes is introduced. Sufficient stability conditions for such a family of schemes are then deduced through the determination of an energy balance analogous to that of the model system. Simulation results are presented in Sec. 3.

1 MODEL AND APPROXIMATE FORMS

The linearized Navier-Stokes equations, including Fourier heat conduction, give a good description of linear acoustic wave propagation in a 3D enclosure $\mathcal{D} \subset \mathbb{R}^3$. The system may be written [24], neglecting rotational flow, as

$$\gamma \partial_t \left(p - \zeta \tau \right) = -\rho c^2 \nabla \cdot \mathbf{v} \,, \tag{1a}$$

$$\gamma \zeta \left(\partial_t - c l_h \Delta \right) \tau = \left(\gamma - 1 \right) \partial_t p \,, \tag{1b}$$

$$\rho \left(\partial_t - c l_v \Delta \right) \mathbf{v} = -\nabla p \,. \tag{1c}$$

Here, the field variables are the irrotational part of the particle velocity $\mathbf{v} = \mathbf{v}(\mathbf{x}, t)$, the acoustic pressure $p = p(\mathbf{x}, t)$, and the temperature distribution $\tau = \tau(\mathbf{x}, t)$—all are functions of $\mathbf{x} \in \mathcal{D}$ and time $t \in \mathbb{R}^+ = [0, \infty]$. ∂_t, ∇, $\nabla \cdot$ and Δ represent, respectively, partial differentiation with respect to time, and the 3D gradient, divergence, and Laplacian operations.

The various parameters appearing in Eq. (1) are: the wave speed c, air density ρ, the ratio of specific heats γ, and the pressure increase per unit temperature increase at constant density ζ. The thermal and viscous characteristic lengths l_h and l_v are defined as

$$l_h = \frac{\lambda}{\rho c C_p} \,, \qquad l_v = \frac{4\mu/3 + \eta}{\rho c} \,. \tag{2}$$

Here, μ and η are viscosity and bulk viscosity, respectively, λ is the coefficient of thermal conductivity, and C_p is heat coefficient at constant pressure for a constant unit mass.

For applications in room acoustics, system Eq. (1) may be simplified considerably—particularly in order to yield a model that is suitable for modeling of viscothermal loss effects over large spaces (and not in the acoustic boundary layer, the effects of which are not significant in this context). As a first step, due to the irrotational nature of the particle velocity $\mathbf{v}$, one may introduce the scalar velocity potential via $\mathbf{v} = -\nabla \Psi(\mathbf{x}, t)$. Under further simplifications [21], system Eq. (1) reduces to a second order viscothermal wave equation:

$$\partial_t^2 \Psi = c^2 \Delta \Psi + c \alpha \partial_t \Delta \Psi \,, \tag{3}$$

where

$$\alpha = l_v + \left(\gamma - 1 \right) l_h \,. \tag{4}$$

and required initial conditions are $\Psi(\mathbf{x}, 0) = w_0(\mathbf{x})$ and $\partial_t \Psi(\mathbf{x}, 0)|_{t=0} = w_1(\mathbf{x})$. Under small values of α, as is the case under typical room conditions, the phase velocity and frequency-dependent damping coefficient are virtually unchanged from those of the model system Eq. (1), despite

the various approximations employed in arriving at Eq. (3) from Eq. (1). Eq. (3) leads to a classic power-law absorption where high frequencies experience more attenuation than low frequencies. This model is a first-order approximation to a more general model of relaxation effects in air and is a particularly good match for audible frequencies of interest under typical air conditions in room acoustics settings, in which case α is on the order of 10^{-6} or 10^{-7} m—see [20, 21].

1.1 Energy Balance

Energy analysis techniques are of great use in determining numerical stability conditions for time-dependent schemes under irregular boundary termination. Such methods, in contrast to frequency domain stability analysis techniques (such as that of von Neumann [13]), allow for an approach to more realistic irregular problem geometries. In essence, the idea is to find a non-negative quantity that is either conserved or dissipated, and which serves to bound the state of the system. In some cases, as, for example, for the full system given in Eq. (1), the physical stored energy of the system serves as a positive semi-definite function of the state and thus serves to bound the growth of the state at any time t. Under the various approximations leading to Eq. (3), however, the energetic behavior of the system is obscured, but one may arrive, nonetheless, at a balance of the form:

$$\frac{d}{dt}E_i = -Q_i + B\,, \tag{5}$$

where here, the energy-like function $E_i(t) \geq 0$ is defined by

$$E_i(t) = \iiint_{\mathcal{D}} \frac{\rho}{2c^2}\left(\partial_t \Psi\right)^2 + \frac{\rho}{2}|\nabla\Psi|^2 dV\,, \tag{6}$$

$Q_i(t) \geq 0$ is a damping term incorporating viscothermal effects:

$$Q_i(t) = \iiint_{\mathcal{D}} \frac{\rho\alpha}{c}|\partial_t \nabla\Psi|^2 dV\,, \tag{7}$$

and $B(t)$ is a term representing effects over the room boundary $\partial\mathcal{D}$:

$$B(t) = -\iint_{\partial\mathcal{D}} \tilde{p}\tilde{v}_\perp d\sigma\,. \tag{8}$$

where $\tilde{p}$ and $\tilde{v}_\perp$ are defined as:

$$\tilde{p} = \rho\partial_t\Psi\,, \qquad \tilde{v}_\perp = -\left(1 + \frac{\alpha}{c}\partial_t\right)\left(\mathbf{n}\cdot\nabla\Psi\right)\,, \tag{9}$$

When viscothermal losses are neglected (i.e., when $\alpha = 0$), E_i is precisely the stored energy in the acoustic field, and B represents power inflow at the room boundary. See Fig. 1.

1.2 Boundary Conditions and Passivity

Under the simplifications that led to the viscothermal wave Eq. (3) from Eq. (1), and given that B can be intepreted as a power-like quantity, it makes sense to associate the quantities $\tilde{p}$ and $\tilde{v}_\perp$ to pressure and outward normal velocity, respectively. These associations are exact under lossless conditions (i.e., when $\alpha = 0$), and for α small, $\tilde{p} \approxeq p$ and

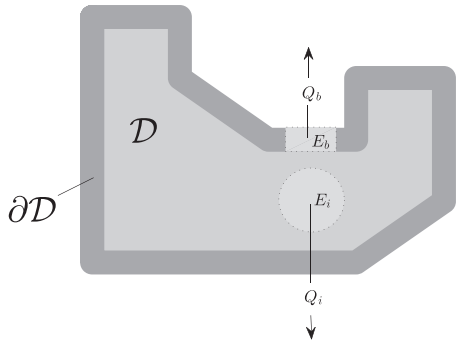

Fig. 1. Room geometry, with interior region $\mathcal{D}$ and the room boundary $\partial\mathcal{D}$. Stored energy E_i and E_b are indicated, as well as power loss Q_i and Q_b.

$\tilde{v}_\perp \approxeq \mathbf{n}\cdot\mathbf{v}$ as would be derived from Eq. (1). Under passive conditions, one must be able to write:

$$B = -Q_b - \frac{d}{dt}E_b \tag{10}$$

for $Q_b(t) \geq 0$, representing wall dissipation, and $E_b(t) \geq 0$, representing stored energy at the wall. Under these conditions, the entire system satisfies an energy balance of the form

$$\frac{dE}{dt} = -Q\,, \tag{11}$$

where $E = E_i + E_b \geq 0$ and $Q = Q_i + Q_b \geq 0$, and the system is dissipative as a whole. The energy balance Eq. (11) implies that, for any $t \geq 0$,

$$\begin{aligned} E(t) - E(0) &= -\int_0^t Q(t')dt' \\ &\Rightarrow\ 0 \leq E(t) \leq E(0)\,. \end{aligned} \tag{12}$$

1.3 A Family of Frequency-Dependent Wall Conditions

One way of satisfying these relationships is by specifying a positive real admittance (in the frequency domain) relating the Laplace-transformed quantities $\tilde{P}(\mathbf{x}, s)$ to $\tilde{V}_\perp(\mathbf{x}, s)$, defined in terms of the complex frequency variable s, and for $\mathbf{x} \in \partial\mathcal{D}$. The admittance relationship is then

$$\tilde{V}_\perp(\mathbf{x}, s) = Y(\mathbf{x}, s)\tilde{P}(\mathbf{x}, s)\,. \tag{13}$$

The admittance Y can be determined through measurement, or through theoretical models of wall materials [17]. Provided that Y is a positive real function [25] of s for all $\mathbf{x} \in \partial\mathcal{D}$, the condition Eq. (13) is a complete characterization of all possible locally-reactive, frequency-dependent, and also spatially-varying passive wall conditions. In order to arrive at a time domain method operating as a recursion, it is a rational approximant that is required. Such a condition ultimately may be written as a differential relationship between $\tilde{p}$ and $\tilde{v}_\perp$, which may be conveniently represented as a one-port circuit element.

It is useful, both for purposes of optimization and implementation, to introduce a tractable subclass of admittances. Using the electrical/acoustical analogy, consider a

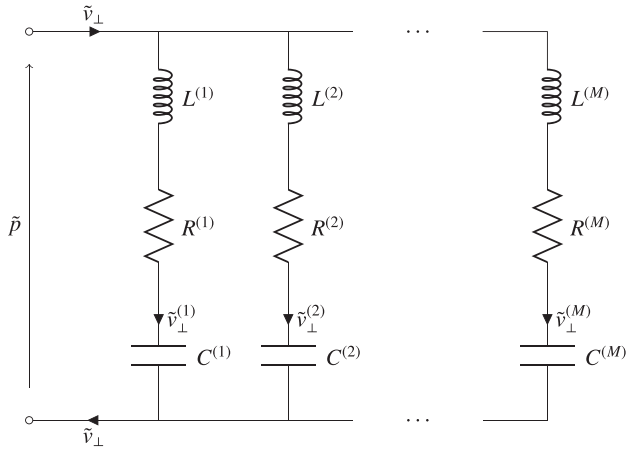

Fig. 2. Parallel-series RLC circuit for general impedance boundary condition

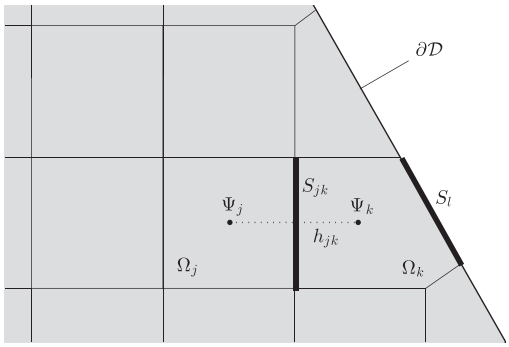

Fig. 3. Finite volume discretization of a domain, shown here in 2D for visibility. Indicated are two cells Ω_j and Ω_k, with inter-cell distance h_{jk}, adjacent surface area S_{jk}, and associated variables Ψ_j and Ψ_k. Cell Ω_k possesses a boundary face, of surface area S_l.

decomposition of the admittance $\hat{Y} \approxeq Y$ into a parallel combination of M series RLC branches, or

$$\hat{Y}(\mathbf{x}, s) = \sum_{m=1}^{M} \frac{s}{L^{(m)}(\mathbf{x})s^2 + R^{(m)}(\mathbf{x})s + \frac{1}{C^{(m)}(\mathbf{x})}}, \qquad (14)$$

where $L^{(m)}(\mathbf{x})$, $R^{(m)}(\mathbf{x})$ and $C^{(m)}(\mathbf{x})$, $m = 1, \ldots, M$ are, respectively, acoustic inductance, resistance, and capacitance for the mth branch and are variable over the room boundary $\partial\mathcal{D}$. See Fig. 2. For passivity, all branch coefficients are constrained to be non-negative everywhere, and $C^{(m)}(\mathbf{x}) > 0$ enforces zero admittance at DC. The decomposition of Y into a sum allows for relatively independent control over the placement of specific wall resonances. See [17, Section V] for more on the topic of fitting $(L^{(m)}, C^{(m)}, R^{(m)})$ parameters to arbitrary complex impedances.

In the time domain, using definition Eq. (14) for the admittance Y, the frequency-domain relationship Eq. (13) may be written, in terms of the additional variables $\tilde{v}_\perp^{(m)}$ and $g^{(m)}$, $m = 1, \ldots, M$, as

$$\begin{aligned}
&\tilde{v}_\perp = \sum_{m=1}^{M} \tilde{v}_\perp^{(m)}, \\
&\tilde{p} = R^{(m)}\tilde{v}_\perp^{(m)} + L^{(m)}\frac{d\tilde{v}_\perp^{(m)}}{dt} + \frac{g^{(m)}}{C^{(m)}}, \qquad m = 1, \ldots, M, \\
&\frac{dg^{(m)}}{dt} = \tilde{v}_\perp^{(m)}, \qquad m = 1, \ldots, M. \qquad (15)
\end{aligned}$$

Returning now to the boundary power inflow term $B(t)$, from Eq. (8), using Eq. (15), it may be rewritten as

$$\begin{aligned}
B(t) &= -\sum_{m=1}^{M} \iint_{\partial\mathcal{D}} \tilde{p}\tilde{v}_\perp^{(m)} d\sigma \\
&= -\frac{d}{dt} \underbrace{\sum_{m=1}^{M} \iint_{\partial\mathcal{D}} \frac{L^{(m)}}{2}\left(\tilde{v}_\perp^{(m)}\right)^2 + \frac{1}{2C^{(m)}}\left(g^{(m)}\right)^2 d\sigma}_{E_b} \\
&\quad - \underbrace{\sum_{m=1}^{M} \iint_{\partial\mathcal{D}} R^{(m)}\left(\tilde{v}_\perp^{(m)}\right)^2 d\sigma}_{Q_b}. \qquad (16)
\end{aligned}$$

where it is clear that, provided the wall parameters $L^{(m)}$, $C^{(m)}$, and $R^{(m)}$ are non-negative, that the stored energy at the wall E_b satisfies $E_b \geq 0$ and the power loss Q_b satisfies $Q_b \geq 0$. Thus the system as a whole is passive, from Eq. (11). It is noted that M is permitted to vary as an integer over the boundary surface, but it is written as a constant in the above expression for simplicity.

2 FINITE VOLUME METHODS

Finite volume methods have a long history, particularly in shock modeling [26]. Finite volume methods for lossless acoustic wave propagation in the context of room acoustics were initially studied in [7] for quasi-Cartesian grids, and a more complete presentation was recently given in [16] and [17] for fully unstructured grids, featuring energy-based stability over complex geometries and under frequency-dependent boundary conditions.

In order to derive finite volume methods for this room acoustics model, first consider a tiling of the problem domain $\mathcal{D}$ into polyhedral cells Ω_j, $j = 1, \ldots, N$, derived from a pre-processing meshing step (see, e.g., [27]). The volume of the jth cell is V_j, and the adjoining surface area and distance to a neighboring cell Ω_k are S_{jk} and h_{jk}, respectively, where $S_{jk} = S_{kj}$ and $h_{jk} = h_{kj}$. The inter-cell distances h_{jk} are completely determined by cell-centroids [16] or by specifying an underlying grid of points [28]. Boundary faces (approximated as piecewise-polygonal) are indexed by $l = 1, \ldots, N_b$, where N_b is the number of boundary faces on $\partial\mathcal{D}$, with surface area S_l. In order to associate a boundary face to a cell (possibly many-to-one), an indicator function β_{jl} will be used, taking on the value 1 if the lth boundary face belongs to Ω_j, and zero otherwise. See Fig. 3, illustrating a typical arrangement of regular cells over the domain interior, with irregular fitted cells at the domain boundary.

Beginning from the approximate form Eq. (3), integrating over cell Ω_j, and employing the divergence theorem

leads to the approximation:

$$\frac{V_j}{c^2}\frac{d^2}{dt^2}\Psi_j = \sum_{k=1}^{N}\beta_{jk}S_{jk}\left(1+\frac{\alpha}{c}\frac{d}{dt}\right)(\nabla\Psi)_{jk} - \sum_{l=1}^{N_b}\beta_{jl}S_l\tilde{v}_{\perp,l}\,. \tag{17}$$

Here, Ψ_j, for $j = 1\ldots, N$ is an approximation to Ψ over the jth cell Ω_j, and β_{jk} is an indicator function taking on the value 1 if two cells Ω_j and Ω_k possess an adjoining face, and 0 otherwise. $(\nabla\Psi)_{jk}$ is an approximation to the normal gradient of Ψ across the boundary between Ω_j and Ω_k; given adjoining cells Ω_j and Ω_k, with associated cell-averaged values f_j and f_k, the operator $(\nabla f)_{jk}$ is defined as

$$(\nabla f)_{jk} = \frac{1}{h_{jk}}\left(f_k - f_j\right)\,, \tag{18}$$

and note that $(\nabla f)_{jk} = -(\nabla f)_{kj}$. The nature of the approximation $\tilde{v}_{\perp,l}$ to $\tilde{v}_\perp$ as defined in Eq. (9) at a boundary face is left unspecified for the moment.

2.1 Time Difference and Averaging Operations

The system of ODEs Eq. (17) must be temporally discretized in order to yield a numerical scheme. To this end, introduce the time series Ψ_j^n, representing an approximation to $\Psi_j(t)$ at $t = nT_s$, for integer $n \geq 0$, and where T_s is the time step (and $F_s = 1/T_s$ is the sample rate in audio applications).

For any time series f^n, the forward and backward shift operators e_+ and e_- are defined by

$$e_+ f^n = f^{n+1}\,, \qquad e_- f^n = f^{n-1}\,. \tag{19}$$

Various difference and averaging operators may be defined in terms of these basic shifts. Forward, backward, and centered difference operations, approximating a first time derivative, are defined by

$$\delta_- = \frac{1}{T_s}(1-e_-)\,, \quad \delta_+ = \frac{1}{T_s}(e_+-1)\,, \quad \delta_\circ = \frac{1}{2T_s}(e_+-e_-)\,. \tag{20}$$

Forward, backward, and centered averaging operators may be defined as

$$\mu_- = \frac{1}{2}(1+e_-)\,, \quad \mu_+ = \frac{1}{2}(e_++1)\,, \quad \mu_\circ = \frac{1}{4}(e_++2+e_-)\,. \tag{21}$$

For more flexibility in scheme construction, it is also useful to define parameterized difference and averaging approximations by

$$\mu_\theta = \theta + (1-\theta)\,\mu_\circ\,, \quad \delta_\xi = \xi\delta_- + (1-\xi)\,\delta_\circ\,. \tag{22}$$

Such approximations, parameterized by the real numbers θ and ξ, respectively, allow for implicit families of schemes, as will be seen shortly.

2.2 Identities and Inequalities

Some useful identities involving quadratic forms are:

$$\delta_\circ f^n \delta_+\delta_- f^n = \delta_+\left(\frac{1}{2}\left(\delta_- f^n\right)^2\right)\,, \tag{23a}$$

$$\delta_\circ f^n \mu_\theta f^n = \delta_+\left(\frac{1}{2}\left(\mu_- f^n\right)^2 - \frac{\theta T_s^2}{8}\left(\delta_- f^n\right)^2\right)\,, \tag{23b}$$

$$\delta_\circ f^n \delta_\xi f^n = \left(\delta_\circ f^n\right)^2 - \delta_+\left(\frac{T_s(1-\xi)}{4}\delta_- f^n\right)^2\,. \tag{23c}$$

For the normal gradient operation between cells, as defined in Eq. (18), the following identity holds, for any cell average grid functions f_j and g_j:

$$\sum_{j,k=1}^{N}\beta_{jk}S_{jk}g_j\,(\nabla f)_{jk} = -\frac{1}{2}\sum_{j,k=1}^{N}\beta_{jk}S_{jk}h_{jk}\,(\nabla g)_{jk}\,(\nabla f)_{jk}\,, \tag{24}$$

where the above summation notation is shorthand for a double series. The above identities are essentially discrete forms of the chain rule for differentiation and Gauss' law, see, e.g., [29]. The following inequality (derived in [16]), which is not necessarily tight, is also useful in stability analysis:

$$\sum_{j,k=1}^{N}\beta_{jk}S_{jk}h_{jk}\,(\nabla f)_{jk}^2 \leq \sum_{j,k=1}^{N}\beta_{jk}\frac{4S_{jk}}{h_{jk}}f_j^2\,. \tag{25}$$

2.3 Fully Discrete Finite Volume Scheme

A fully discrete family of finite volume schemes follows from the application of time difference and averaging operators to the semi-discrete form Eq. (17):

$$\frac{V_j}{c^2}\delta_+\delta_-\Psi_j^n = \sum_{k=1}^{N}\beta_{jk}S_{jk}\left(\mu_\theta+\frac{\alpha}{c}\delta_\xi\right)(\nabla\Psi)_{jk}^n - \sum_{l=1}^{N_b}\beta_{jl}S_l\mu_\circ\tilde{v}_{\perp,l}^n\,. \tag{26}$$

Notice that the scheme depends on the two parameterized operators μ_θ and δ_ξ, as defined in Eq. (22), and thus depends globally on two free parameters. In particular, when $\theta = \xi = 1$, the scheme is fully explicit. Otherwise, the scheme is implicit and requires a linear system to be solved at each time-step, where the additional cost associated to the (sparse) linear system solution using iterative methods [30] will strongly depend on the choice of θ, and to a lesser extent ξ, since α will be small.

The approximation $\tilde{v}_{\perp,l}^n$ follows from the continuous time Eqs. (15). Making use of the bilinear transform as a

temporal discretization rule at the boundaries leads to:

$$\tilde{v}^n_{\perp,l} = \sum_{m=1}^{M_l} \tilde{v}^{(m),n}_{\perp,l} ,$$
$$\rho\delta_\circ \Psi^n_j = R^{(m)}_l \mu_\circ \tilde{v}^{(m),n}_{\perp,l} + L^{(m)}_l \delta_\circ \tilde{v}^{(m),n}_{\perp,l} + \frac{1}{C^{(m)}_l} \mu_\circ g^{(m),n}_l ,$$
$$\delta_\circ g^{(m),n}_l = \mu_\circ \tilde{v}^{(m),n}_{\perp,l} , \quad (27)$$

where $\tilde{v}^n_{\perp,l}$ is a wall velocity at a boundary face l adjoining cell Ω_j, and where the latter two equations hold for $m = 1, \ldots, M_l$. The constants $L^{(m)}_l$, $R^{(m)}_l$ and $C^{(m)}_l$, again non-negative, are the acoustic inductance, resistance and capacitance, for the mth branch, $m = 1, \ldots, M_l$ over boundary face l, $l = 1, \ldots, N_b$. $g^{(m)}_l$ and $\tilde{v}^{(m)}_{\perp,l}$ are auxiliary variables defined at branch m, $m = 1, \ldots, M_l$ and over boundary face l, $l = 1, \ldots, N_b$. Note that extra state is required at the boundaries as is natural for any frequency-dependent boundary condition. The full implicit/explicit update recursion is provided in the Appendix.

Fully-discrete approximations to the pressure field and vector velocity components can be recovered from Ψ^n_j using the following approximations to Eq. (9):

$$\tilde{p}^{n+1/2}_j = \rho\delta_+ \Psi^n_j , \quad \tilde{v}^n_{jk} = -\left(\mu_\theta + \frac{\alpha}{c}\delta_\xi\right)(\nabla\Psi)^n_{jk} . \quad (28)$$

If so desired, an equivalent second-order scheme in terms of pressure variables $\tilde{p}^{n+1/2}_j$ (rather than Ψ^n_j) can be obtained simply by applying $\rho\delta_+$ to both sides of Eqs. (26) and (27) and making use of the above substitution for $\tilde{p}^{n+1/2}_j$. An equivalent first-order scheme in terms of the staggered variables $\tilde{p}^{n+1/2}_j$ and $\tilde{v}^n_{jk}$ is also possible, but it is less efficient than the second-order scheme and thus left out for brevity.

2.4 Energy Balance

In order to arrive at an energy balance analogous to Eq. (5), multiply Eq. (26) by $\rho\delta_\circ \Psi^n_j$ and sum over all cells. Employing identities Eqs. (23) and (24) leads to:

$$\delta_+ E^{n-1/2} = -Q^n . \quad (29)$$

Here, the energy-like quantity $E^{n-1/2}$ and power loss Q^n may be separated into contributions over the problem interior and over the boundary as

$$E^{n-1/2} = E^{n-1/2}_i + E^{n-1/2}_b , \quad Q^n = Q^n_i + Q^n_b . \quad (30)$$

The stored energy terms are defined as follows:

$$E^{n-1/2}_i = \sum_{j=1}^{N} \frac{\rho V_j}{2c^2}\left(\delta_- \Psi^n_j\right)^2 + \sum_{j,k=1}^{N} \beta_{jk} \frac{\rho S_{jk} h_{jk}}{4}\left(\mu_- (\nabla\Psi)^n_{jk}\right)^2 - \left(\frac{T_s\theta}{2} + \frac{\alpha\xi}{c}\right) \times \sum_{j,k=1}^{N} \beta_{jk} \frac{\rho T_s S_{jk} h_{jk}}{8}\left(\delta_- (\nabla\Psi)^n_{jk}\right)^2 , \quad (31)$$

$$E^{n-1/2}_b = \sum_{l=1}^{N_b}\sum_{m=1}^{M_l} \frac{\rho S_l}{2} \times \left(L^{(m)}_l \left(\mu_- v^{(m),n}_{\perp,l}\right)^2 + \frac{\left(\mu_- g^{(m),n}_l\right)^2}{C^{(m)}_l} \right) . \quad (32)$$

The loss terms are defined as

$$Q^n_i = \sum_{j,k=1}^{N} \beta_{jk} \frac{\rho\alpha S_{jk} h_{jk}}{2c}\left(\delta_\circ (\nabla\Psi)^n_{jk}\right)^2 , \quad (33)$$

$$Q^n_b = \sum_{l=1}^{N_b}\sum_{m=1}^{M_l} \rho S_l R^{(m)}_l \left(\mu_\circ v^{(m),n}_{\perp,l}\right)^2 . \quad (34)$$

2.5 Stability

For stability, we require that both $Q^n \geq 0$, and $E^{n-1/2} \geq 0$. Under these conditions, it is true, from Eq. (29), that the energy function is monotonically decreasing and thus available to bound the state. In other words,

$$0 \leq E^{n-1/2} \leq E^{1/2} , \quad (35)$$

where $E^{1/2}$ is the initial energy of the system, calculated from Ψ^n_j at times steps $n = 0$ and $n = 1$.

From the expressions above for Q^n_i and Q^n_b, non-negativity of Q^n is obvious. The analysis of $E^{n-1/2}$ may be neatly subdivided into an examination of the scheme over the interior and over the boundary—indeed, this is one of the main benefits of a finite volume approach. $E^{n-1/2}_b$ is non-negative by construction, but $E^{n-1/2}_i$ is not necessarily. Stability analysis thus reduces to the determination of non-negativity conditions for this term.

Note first that if $\theta \leqslant 0$ and $\xi \leqslant 0$, then $E^{n-1/2}_b$ is non-negative, and the scheme is unconditionally stable (when $\theta = \xi = 0$, the trapezoid rule results). Though this scheme is implicit, and thus requires a linear system solution at each time-step, for a given sample rate it may be used without restriction on the sizes of cells in the tiling (or equivalently, without restriction on the time-step for a given tiling).

Stability analysis for the case of $\theta > 0$ and $\xi > 0$ (which includes the explicit scheme with $\theta = \xi = 1$) is more delicate. Using Eq. (25), one may bound $E^{n-1/2}_i$ as

$$E^{n-1/2}_i \geq \sum_{j=1}^{N} \frac{\rho}{2c^2} V_j \kappa_j \left(\delta_- \Psi^n_j\right)^2 , \quad (36)$$

where

$$\kappa_j = 1 - \left(\frac{c^2 T_s^2 \theta}{2} + c T_s \alpha\xi\right) \sum_{k=1}^{N} \beta_{jk} \frac{S_{jk}}{V_j h_{jk}} . \quad (37)$$

The condition $\kappa_j \geq 0$, for $j = 1, \ldots, N$, thus serves as a locally-verifiable sufficient stability condition for the scheme, at every cell Ω_j. For Cartesian cells in 3D, for

example, where $h_{jk} = h$, $S_{jk} = h^2$ and $V_j = h^3$, the condition reduces to

$$cT_s \leq \sqrt{\frac{h^2}{3\theta} + \left(\frac{\alpha\xi}{\theta}\right)^2} - \frac{\alpha\xi}{\theta}\,, \tag{38}$$

which, from von Neumann analysis, is also the necessary condition for the scheme on the interior domain (for $\theta > 0$ and $\xi > 0$). For the regular arrangements of cells, the sufficient condition Eq. (37) and the von Neumann condition for the FDTD scheme do not always coincide [17]. In particular, when the cell is composed of rhombic dodecahedra (see Fig. 6) with $h_{jk} = h$, $S_{jk} = h^2/(2\sqrt{2})$ and $V_j = h^3/\sqrt{2}$ [19], the von Neumann condition is:

$$cT_s \leq \sqrt{\frac{h^2}{2\theta} + \left(\frac{\alpha\xi}{\theta}\right)^2} - \frac{\alpha\xi}{\theta}\,. \tag{39}$$

Stability conditions for the entire scheme can also be obtained through direct analysis of the non-negativity of Eq. (31), which is made practical for such large sparse systems through the use of standard eigenvalue solvers (e.g., [31]).

2.6 Integrated Energy Balance

For the purposes of verification of the energy balance Eq. (29), it is useful to define the time integrated energy losses in the boundary and over the interior as

$$E^{n-1/2}_{b,loss} = T_s \sum_{\nu=1}^{n-1} Q^{\nu}_b\,, \qquad E^{n-1/2}_{i,loss} = T_s \sum_{\nu=1}^{n-1} Q^{\nu}_i\,. \tag{40}$$

The energy balance Eq. (5) may then be written, at any time step n, as

$$E^{n-1/2}_{balance} = E^{n-1/2} + E^{n-1/2}_{b,loss} + E^{n-1/2}_{i,loss} = \text{constant} \geq 0\,. \tag{41}$$

3 NUMERICAL RESULTS

Simulation results are presented in this section with the intention of illustrating both features of the model system, including both wall absorption and viscothermal losses, as well as numerical features such as the maintenance of a numerical energy balance. For the following simulations, $c = 340$ m/s and $\rho = 1.2$ kg/m^3.

3.1 A Cubic Room Under Rigid-Wall Conditions, With and Without Viscothermal Losses

As an elementary example, consider a cubic room, of side length 4 m. Scheme Eq. (26) is used with $\theta = \xi = 1$ (fully explicit), at a sample rate of 44.1 kHz, and over a regular Cartesian grid (congruent cubic cells). The scheme is excited by the initial conditions $w_0 = 0$ and $w_1 = V_0 c^2 \delta(\mathbf{x} - \mathbf{x}_0)$ with $\mathbf{x}_0$ a position near the center of the room and where V_0 is a reference volume, and T_s set at the stability limit Eq. (38). Output spectra of one-second responses—filtered with a DC-blocker [32] and normalized by the reference volume V_0, for clarity—are shown in Fig. 4, illustrating the response under perfectly reflective conditions without viscothermal losses ($\alpha = 0$, fully lossless) and with viscothermal losses

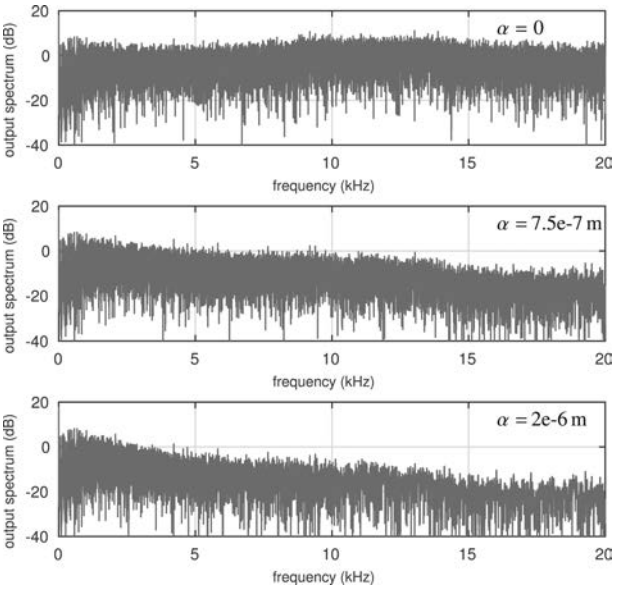

Fig. 4. Output spectra for responses within a cubic room under perfectly reflective boundary termination, with and without viscothermal losses (with α as specified above).

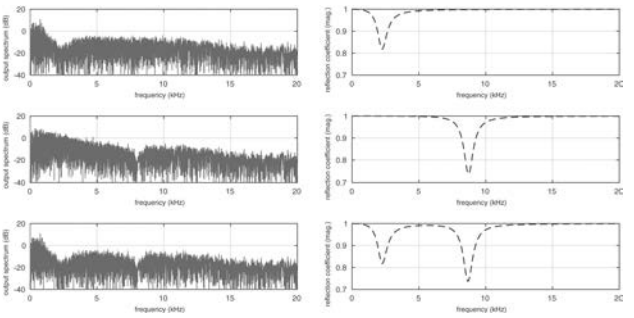

Fig. 5. Output spectra (left) for a response within a cubic room under frequency-dependent boundary terminations and viscothermal losses (α = 2e-6 m), and frequency-dependent reflection coefficient magnitudes for boundary terminations (right). Top: single branch, $(L, R, 1/C) = \rho c$(2e-4, 0.2, 4e4). Middle: single branch (L, R, $1/C$) = ρc(2e-4, 0.15, 6e5). Bottom: two branches, $(L^{(1)}, R^{(1)}, 1/C^{(1)}) = \rho c$(2e-4, 0.2, 4e4) and $(L^{(2)}, R^{(2)}, 1/C^{(2)}) = \rho c$(2e-4, 0.15, 6e5).

($\alpha > 0$). As expected, the presence of viscothermal losses leads to a tilt in the overall response in comparison to the fully lossless case, with the tilt steepening for higher α. The values of α chosen for Fig. 4, α = 7.5e-7 m and α = 2e-6 m, pertain approximately to 80% and 40% relative humidities at 15°C [21].

3.2 A Cubic Room Under Frequency-Dependent Wall Conditions With Viscothermal Losses

Consider again the cubic room using the same scheme and excitation, with viscothermal losses (α = 2e-6 m), and under frequency-dependent wall terminations. Three examples are presented in Fig. 5, corresponding to wall conditions of the form Eq. (15) with single- or multi-branch (L, R, C) coefficients as specified in the figure caption. Output spectra are shown along frequency-dependent reflection

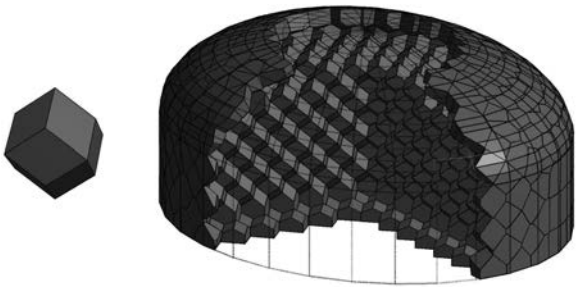

Fig. 6. Left: a rhombic dodecahedron, the Voronoi cell of the FCC grid. Right: a partial tiling of a nontrivial room geometry, with a tiling of rhombic dodecahedra over the interior combined with cells fitted to the room boundary.

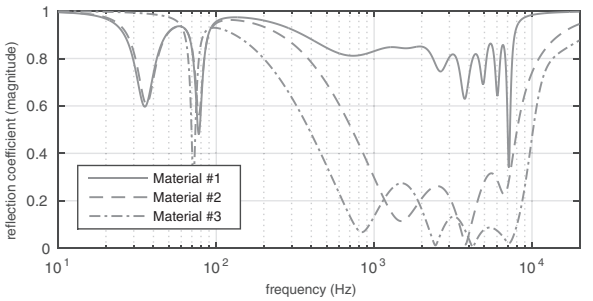

Fig. 7. Frequency-dependent reflection coefficient magnitudes for three wall materials (for $L^{(m)}$, $R^{(m)}$, $C^{(m)}$ branch coefficients, see [17, Table II]).

coefficients (magnitude only) in Fig. 5 and a general correspondence is observed in all cases. One may observe a slight mismatch between theoretical wall resonances and output responses, this is due in small part to numerical dispersion [15], but also due to frequency warping inherent in the underlying bilinear transform [32]—more will be said about this in Sec. 4.

3.3 A Nontrivial Room Geometry

As a more realistic example, consider the elliptical domed geometry illustrated in Fig. 6. Here it is clear that, if a regular tiling is used, some sort of fitting of cells must occur at the boundaries—in the case of the geometry in Fig. 6, a rhombic dodecahedral tiling is employed, corresponding, over the interior, to the use of an FDTD scheme over a FCC grid [19]. The importance of using fitted cells cannot be underestimated, when compared with, e.g., a crude staircased approximation, as employed by various authors [12]. Though room mode frequencies may be consistently approximated with such a staircased termination, room decay times can be grossly underestimated (as shown in [17]), for the simple reason that the bounding surface area of the room is too large, and will remain so even in the limit of small cells. The use of fitted cells corrects for this anomalous behavior and furthermore yields a more accurate approximation to the mode frequencies [17].

For this example, boundary conditions are set to model three different wall materials that might be found in a typical room acoustics scenario. The $L^{(m)}$, $R^{(m)}$, $C^{(m)}$ branch coefficients for these materials were presented in [17, Section V] (omitted here for brevity), and these materials require up to nine branches. The reflection coefficients for Materials #1–3 are illustrated in Fig. 7. Material #3 is applied to the elliptical floor of the room, Material #2 is applied to the walls perpendicular to the floor, and Material #1 to the remainder of the boundary surfaces (the elliptical dome). The viscothermal losses are set to $\alpha = 2\text{e-}6$ m.

Snapshots of the time evolution of the acoustic field in this room geometry are shown in Fig. 8, resulting from initial conditions w_0 being a spatial Gaussian centered about the interior of the room and with variance 0.1 m^2, and $w_1 = 0$. Here, the explicit scheme has been used ($\theta = \xi = 1$) at a sample rate of 4 kHz. As a test of the energy balanced property of the scheme, the individual components

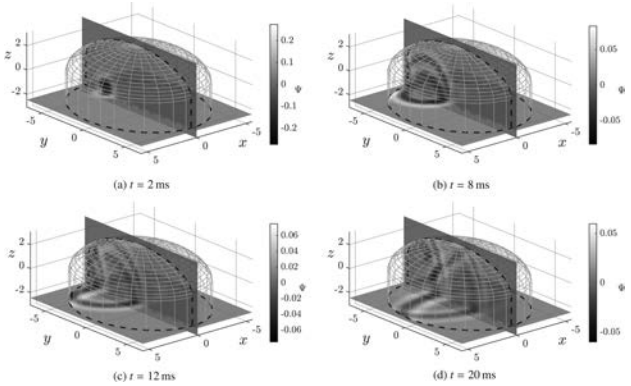

Fig. 8. Snapshots of the time evolution of the acoustic field, at times as indicated, subject to an initial pulse. The sample rate here is 4 kHz and the FCC interior grid spacing is $h = 12$ cm ($cT_s/h \approx 0.7$). The initial displacement here is a spatial Gaussian with variance 0.1 m^2. Axes are in units of metres.

of the energy balance are plotted in Fig. 9, along with the normalized energy variation, illustrating a numerical energy balance valid near the limit of machine precision (see [33] for a discussion of round-off effects in energy calculations). The test problem is carried out with the same mesh, but for two choices ξ and θ that lead to implicit schemes, where the linear systems involved are solved using standard iterative techniques [30, 34]. Fig. 10 shows the energy variations from these simulations, which are again on the order of machine accuracy.

Another useful feature of the use of fitted cells at boundaries is that the finite volume approximation tends to converge to the unique solution of this room acoustics model for a given set of initial conditions [17]—the same cannot be said of other wave-based approaches that suffer from staircasing errors (such as, e.g., [15, 12, 11]), as such errors do not disappear in the limit of small cell sizes [17]. As a result, this FVTD approach may be used to compute reference solutions for the room acoustics model under examination. One such reference solution is displayed in Fig. 11, which was computed on a sufficiently refined grid to be able to ignore dispersion effects for the scheme and chosen initial conditions. Fig. 12 shows residual signals from outputs computed on coarser grids (lower sample rates). As can be seen, the residual energy tends to decrease with grid

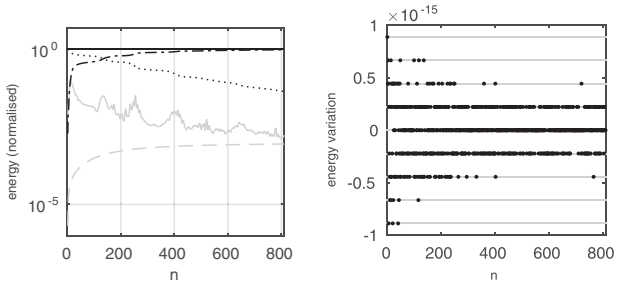

Fig. 9. Left: Energy balance corresponding to the simulation shown in Fig. 8. Here, the solid black line represents the total integrated energy $E^{n-1/2}_{balance}$ from Eq. (41), which is constant, as expected. Also displayed are the total stored energy in the acoustic field $E^{n-1/2}_{i}$ (dotted), the total stored energy at the boundary $E^{n-1/2}_{b}$ (solid grey), the integrated power loss over the interior $E^{n-1/2}_{i,loss}$ (dashed), and the integrated power loss $E^{n-1/2}_{b,loss}$ at the boundary (dash-dotted). Right: instantaneous normalized variation in $E^{n-1/2}_{balance}$, defined as $(E^{n+1/2}_{balance} - E^{n-1/2}_{balance})/2^{\lfloor \log_2 E^{1/2}_{balance} \rfloor}$. Grey lines are integer multiples of machine epsilon (2^{-52}).

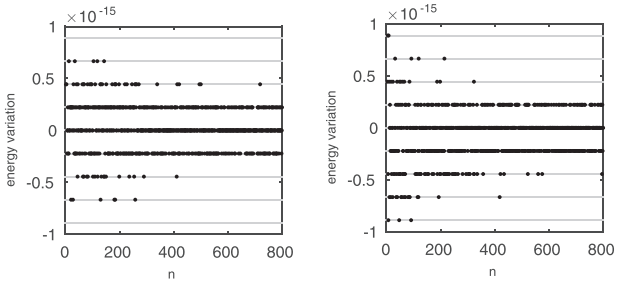

Fig. 10. Instantaneous normalized variations in $E^{n-1/2}_{balance}$ for implicit schemes. Left: $\theta = 0$, $\xi = 1$. Right: $\theta = 0$, $\xi = 0$. Grey lines are integer multiples of machine epsilon (2^{-52}).

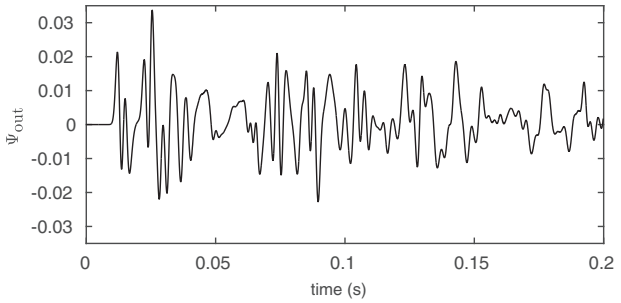

Fig. 11. Output from simulation run with $F_s = 10$ kHz, with FCC interior grid spacing $h = 4.8$ cm ($cT_s/h \approx 0.7$) and fitted cells at boundaries. The initial displacement here is a spatial Gaussian with variance 0.1 m^2.

refinement, suggesting that the scheme is indeed convergent. Finally, a higher-bandwidth solution is computed for one second output and displayed in Fig. 13.

4 CONCLUDING REMARKS

The main focus of this paper has been the illustration of construction techniques for wave-based simulation methods for nontrivial problems in room acoustics, including irregular geometries, frequency-dependent boundary conditions, extended to include viscothermal loss effects in air. Finite volume methods have been employed, here in both Cartesian and FCC forms, as they reduce to (and may be programmed as) simple FDTD methods over the problem interior but allow for a complete analysis of boundary termination for such schemes. As has been seen, the addition of viscothermal loss does not introduce any undue complications in this regard. Indeed, a family of schemes has been presented, including both explicit and implicit members, and has been shown to satisfy an energy balance, including time-integrated power loss over both the room interior and at the wall termination, to near machine precision.

The viscothermal loss model presented here is a good first approximation, but neglects some relaxation effects [21, 20], which complicates the frequency dependence of the model, and, ultimately, the approximation method. It would be of interest to include such effects in a more refined model. That being said, a larger effect is almost

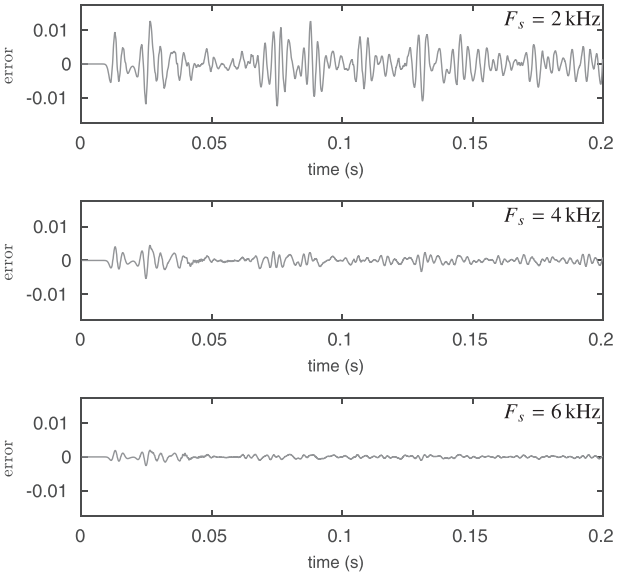

Fig. 12. Output errors of simulations run at sample rates specified above, using a FCC grid over the problem interior (with $cT_s/h \approx 0.7$) and fitted cells at boundaries. The initial displacement here is a spatial Gaussian with variance 0.1 m^2.

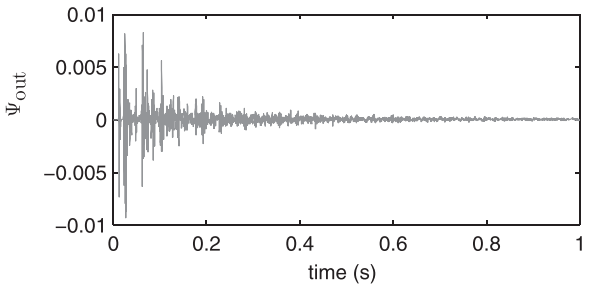

Fig. 13. Output from simulation run at 10 kHz with FCC interior grid spacing $h = 4.8$ cm ($cT_s/h \approx 0.7$) and fitted cells at boundaries. The initial displacement here is a spatial Gaussian with variance 0.01 m^2.

certainly inaccuracy in the discrete approximation in terms of numerical decay constants. This is a more difficult matter, at least in the present context, as the stability analysis here relies on the local interconnection of nearest-neighbor cells. A correspondence with wider stencil (and potentially more accurate, but no longer local, and more difficult to analyze) implicit and explicit FDTD schemes (e.g., [35, 36, 34]) will be the subject of future study. A further numerical issue is the warping of the frequency-dependence of the numerical absorption at boundaries, due to the particular choice of the bilinear transform as a temporal discretization rule. A possible avenue of approach might be optimizing of discrete branch coefficients according to pre-warped frequencies, as is commonly used in digital filter design [32].

5 ACKNOWLEDGMENT

This work was supported by the European Research Council, under grant number ERC-StG-2011-279068-NESS.

6 REFERENCES

[1] V. Välimäki, J. D. Parker, L. Savioja, J. O.III Smith, and J. S. Abel "Fifty Years of Artificial Reverberation," *IEEE Trans. Audio, Speech, and Language Processing*, vol. 20, no. 5, pp. 1421–1448 (2012).

[2] L. Savioja "Real-Time 3D Finite-Difference Time-Domain Simulation of Low- and Mid-Frequency Room Acoustics," *Proc. Digital Audio Effects (DAFx)*, vol. 1, p. 75 (Graz, Austria) (2010).

[3] C. J. Webb and A. Gray "Large-Scale Virtual Acoustics Simulation at Audio Rates Using Three Dimensional Finite Difference Time Domain and Multiple GPUs," *Proc. Int. Cong. Acoustics (ICA)* (Montréal, Canada) (2013).

[4] G. E. Forsythe and W. R. Wasow *Finite-Difference Methods for Partial Differential Equations* (New York: Wiley, 1960).

[5] L. Savioja, T. J. Rinne, and T. Takala "Simulation of Room Acoustics with a 3-D Finite Difference Mesh," *Proc. Int. Computer Music Conf. (ICMC)*, pp. 463–466, Danish Institute of Electroacoustic Music, Denmark (1994).

[6] O. Chiba, T. Kashiwa, H. Shimoda, S. Kagami, and I. Fukui "Analysis of Sound Fields in Three Dimensional Space by the Time-Dependent Finite-Difference Method Based on the Leap Frog Algorithm," *J. Acoust. Soc. Jpn.(J)*, vol. 49, pp. 551–562 (1993).

[7] D. Botteldooren "Acoustical Finite-Difference Time-Domain Simulation in a Quasi-Cartesian Grid," *J. Acous. Soc. Amer.*, vol. 95, no. 5, pp. 2313–2319 (1994).

[8] S. Bilbao *Wave and Scattering Methods for Numerical Simulation* (John Wiley and Sons, Chichester, UK, 2004).

[9] G. R. Campos and D. M. Howard "On the Computational Efficiency of Different Waveguide Mesh Topologies for Room Acoustic Simulation," *IEEE Trans. Speech and Audio Processing*, vol. 13, no. 5, pp. 1063–1072 (2005).

[10] S. Nakamoto "Phase-Error Analysis of High-Order Finite Difference Time Domain Scheme and its Influence on Calculation Results of Impulse Response in Closed Sound Field," *Acous. Sci. & Tech.*, vol. 28, no. 5, pp. 295–309 (2007).

[11] M. Hornikx, T. Krijnen, and L. van Harten, "openPSTD: The Open Source Pseudospectral Time-Domain Method for Acoustic Propagation," *Computer Physics Communications*, vol. 203, pp. 298-308 (2016).

[12] N. Morales, R. Mehra, and D. Manocha "A Parallel Time-Domain Wave Simulator Based on Rectangular Decomposition for Distributed Memory Architectures," *Applied Acoustics*, vol. 97, pp. 104–114 (2015).

[13] J. Strikwerda *Finite Difference Schemes and Partial Differential Equations* (SIAM, Philadelphia, PA, 2004).

[14] K. Kowalczyk and M. van Walstijn "Modeling Frequency-Dependent Boundaries as Digital Impedance Filters in FDTD and K-DWM Room Acoustics Simulations," *J. Audio Eng. Soc.*, vol. 56, pp. 569–583 (2008 Jul./Aug.).

[15] K. Kowalczyk and M. van Walstijn "Room Acoustics Simulation Using 3-D Compact Explicit FDTD Schemes," *IEEE Trans. Audio, Speech, and Language Processing*, vol. 19, no. 1, pp. 34–46 (2011).

[16] S. Bilbao "Modeling of Complex Geometries and Boundary Conditions in Finite Difference/Finite Volume Time Domain Room Acoustics Simulation," *IEEE Trans. Audio, Speech, and Language Processing*, vol. 21, no. 7, pp. 1524–1533 (2013 Jul.).

[17] S. Bilbao, B. Hamilton, J. Botts, and L. Savior "Finite Volume Time Domain Room Acoustics Simulation under General Impedance Boundary Conditions," *IEEE/ACM Trans. Audio, Speech, and Language Processing*, vol. 24, no. 1, pp. 161–173 (2016).

[18] T. Sakuma, S. Sakamoto, and T. Otsuru *Computational Simulation in Architectural and Environmental Acoustics* (Springer Japan, 2014), pp. 133–140.

[19] B. Hamilton and C. J. Webb "Room Acoustics Modelling Using GPU-Accelerated Finite Difference and Finite Volume Methods on a Face-Centered Cubic Grid," *Proc. Digital Audio Effects (DAFx)*, pp. 336–343, Maynooth, Ireland (2013 Sep.).

[20] A. D. Pierce *Acoustics: An Introduction to its Physical Principles and Applications* (McGraw-Hill New York, 1989).

[21] B. Hamilton, S. Bilbao, and C. J. Webb "Improved Finite Difference Schemes for a 3-D Viscothermal Wave Equation on a GPU," *Proceedings of Forum Acusticum*, Krakow, Poland (2014).

[22] J. Botts and L. Savioja "Extension of a Spectral Time-Stepping Domain Decomposition Method for Dispersive and Dissipative Wave Propagation," *J. Acous. Soc. Amer.*,vol. 137, no. 4, pp. EL267–EL273 (2015).

[23] S. Bilbao and B. Hamilton "Finite Volume Modeling of Viscothermal Losses and Frequency-Dependent Boundaries in Room Acoustics Simulations," presented at the *AES 60th International Conference: DREAMS (Dereverberation and Reverberation of Audio, Music, and Speech)* (2016 Jan.), conference paper 5-3.

[24] M. Bruneau, P. Herzog, J. Kergomard, and J.D. Police "General Formulation of the Dispersion Equation in

Bounded Visco-Thermal Fluid, and Application to Some Simple Geometries," *Wave Motion*, vol. 11, no. 5, pp. 441–451 (1989).

[25] L. Weinberg *Network Analysis and Synthesis* (McGraw-Hill, New York, NY, 1962).

[26] R. J. LeVeque *Finite Volume Methods for Hyperbolic Problems*, vol. 31 (Cambridge University Press, Cambridge, UK, 2002).

[27] J. F. Thompson, B. K. Soni, and N. P. Weatherill *Handbook of Grid Generation* (CRC Press, 1998).

[28] B. Hamilton "Finite Volume Perspectives on Finite Difference Schemes and Boundary Formulations for Wave Simulation," *Proc. Digital Audio Effects (DAFx)*, Erlangen, Germany (2014 Sep.).

[29] S. Bilbao *Numerical Sound Synthesis: Finite Difference Schemes and Simulation in Musical Acoustics* (Wiley, 2009).

[30] Y. Saad *Iterative Methods for Sparse Linear Systems* (SIAM, 2003).

[31] R. R. B. Lehoucq, D. D. C. Sorensen, and C.-C. Yang *ARPACK User's Guide: Solution of Large-Scale Eigenvalue Problems with Implicitly Restorted Arnoldi Methods*, vol. 6 (SIAM, 1998).

[32] J. O., Smith III *Introduction to Digital Filters: With Audio Applications*, vol. 2 (W3K Publishing, 2007).

[33] A. Torin, *Percussion Instrument Modelling in 3D: Sound Synthesis Through Time Domain Numerical Simulation*. Ph.D. thesis, University of Edinburgh (2016).

[34] B. Hamilton, S. Bilbao, and C. J. Webb "Revisiting Implicit Finite Difference Schemes for 3-D Room Acoustics Simulations on GPU," *Proc. Digital Audio Effects (DAFx)*, Erlangen, Germany (2014).

[35] K. Kowalczyk and M. van Walstijn "A Comparison of Nonstaggered Compact FDTD Schemes for the 3D Wave Equation," *Proc. IEEE ICASSP*, pp. 197–200, Dallas, Texas (2010).

[36] S. Bilbao "Optimized FDTD Schemes for 3-D Acoustic Wave Propagation," *IEEE Trans. Audio, Speech, and Language Processing*, vol. 20, no. 5, pp. 1658–1663 (2012).

APPENDIX

Given a tiling (mesh) of the domain, the implementation of the scheme is as follows. From initial conditions $\Psi(\mathbf{x}, 0) = w_0(\mathbf{x})$ and $\partial_t \Psi(\mathbf{x}, 0)|_{t=0} = w_1(\mathbf{x})$, the scheme can be initialised with:

$$\Psi_j^0 = [w_0]_j\,, \quad \Psi_j^1 = [w_0]_j + T_s[w_1]_j\,.$$

where $[w_0]_j$ denotes $w_0(\mathbf{x})$ averaged over cell Ω_j. The following definitions will also be helpful:

$$W_j^n = \sum_{k=1}^{N} \frac{\beta_{jk} S_{jk}}{V_j h_{jk}} (\Psi_k^n - \Psi_j^n)\,,$$

$$\bar{v}_l^{(m),n-1/2} = \mu_- \tilde{v}_{\perp,l}^{(m),n}\,, \quad \bar{g}_l^{(m),n-1/2} = \mu_- g_l^{(m),n}\,,$$

$$\tau_l^{(m)} = \left(\frac{L_l^{(m)}}{T_s} + \frac{R_l^{(m)}}{2} + \frac{T_s}{4C_l^{(m)}} \right)^{-1}\,.$$

For $n > 1$, the time-stepping update for the implicit/explicit scheme is carried out in three steps.

(Step 1) Calculate the temporary variable:

$$\begin{aligned}\Psi_j^\star = {} & 2\Psi_j^n - \Psi_j^{n-1} + \frac{1}{2}\left((\theta+1)c^2T_s^2 + 2cT_s\alpha\xi\right) W_j^n \\ & - \frac{1}{4}\left((\theta-1)c^2T_s^2 + 2cT_s\alpha(1+\xi)\right) W_j^{n-1} \\ & - \frac{c^2T_s^2}{2V_j} \sum_{l=1}^{N_b} \sum_{m=1}^{M_l} \gamma_{jl} S_l \tau_l^{(m)} \\ & \times \left(\frac{2L_l^{(m)} \bar{v}_l^{(m),n-1/2}}{T_s} - \frac{\bar{g}_l^{(m),n-1/2}}{C_l^{(m)}} - \frac{\rho \Psi_j^{n-1}}{2T_s} \right).\end{aligned}$$

(Step 2) Solve the linear system ($j = 1, \ldots, N$):

$$\begin{aligned}& \frac{1}{4}\left((\theta-1)c^2T_s^2 + 2cT_s\alpha(\xi-1)\right) W_j^{n+1} \\ & + \left(1 + \frac{\rho c^2 T_s}{4V_j} \sum_{l=1}^{N_b} \sum_{m=1}^{M_l} \gamma_{jl} S_l \tau_l^{(m)}\right) \Psi_j^{n+1} = \Psi_j^\star\,.\end{aligned}$$

(Step 3) Update the boundary quantities with:

$$\begin{aligned}\bar{v}_l^{(m),n+1/2} = {} & \tau_l^{(m)} \left(\left(\frac{L_l^{(m)}}{T_s} - \frac{R_l^{(m)}}{2} - \frac{T_s}{4C_l^{(m)}} \right) \bar{v}_l^{(m),n-1/2} \right. \\ & \left. - \frac{\bar{g}_l^{(m),n-1/2}}{C_l^{(m)}} + \frac{\rho}{2T_s} \sum_{j=1}^{N} \gamma_{jl} \left(\Psi_j^{n+1} - \Psi_j^{n-1} \right) \right)\,,\end{aligned}$$

$$\bar{g}_l^{(m),n+1/2} = \frac{T_s}{2}\left(\bar{v}_l^{(m),n+1/2} + \bar{v}_l^{(m),n-1/2} \right) + \bar{g}_l^{(m),n-1/2}\,.$$

In the explicit case ($\theta = \xi = 1$), the linear system to solve is diagonal and one can combine Steps 1 and 2. In terms of memory storage, the explicit update can be carried out using three states of size N: Ψ_j^{n+1}, Ψ_j^n, and Ψ_j^{n-1}; and $3M_l$ additional states per boundary face $l = 1, \ldots, N_b$: $\bar{v}_l^{(m),n+1/2}$, $\bar{v}_l^{(m),n-1/2}$, and $\bar{g}_l^{(m),n-1/2}$. Note that in Step 3, $\bar{g}_l^{(m),n+1/2}$ can overwrite $\bar{g}_l^{(m),n-1/2}$ in place. The implicit scheme requires at least one additional state of size N.

THE AUTHORS

Stefan Bilbao

Brian Hamilton

Stefan Bilbao (B.A. physics, Harvard, 1992, M.Sc., Ph.D. electrical engineering, Stanford, 1996 and 2001 respectively) is currently a Reader in the Acoustics and Audio Group at the University of Edinburgh and was previously a lecturer at the Sonic Arts Research Centre, at the Queen's University Belfast, and a research associate at the Stanford Space Telecommunications and Radioscience Laboratories. He is currently the leader of the NESS project (Next Generation Sound Synthesis), funded by the European Research Council, and running jointly between the Acoustics and Audio Group and the Edinburgh Parallel Computing Centre at the University of Edinburgh between 2012 and 2017.

•

Brian Hamilton received B.Eng. (Hons) and M.Eng. degrees in electrical engineering from McGill University in Montréal, QC, Canada, in 2009 and 2012, respectively, and his Ph.D. from the University of Edinburgh in 2016. He is currently a postdoctoral research fellow in the Acoustics and Audio group at the University of Edinburgh. His research interests include numerical methods for 3-D room acoustics simulations and spatial audio.